Korean J. Chem. Eng., 34(7), 2019-2026 (2017)
DOI: 10.1007/s11814-017-0103-4

pISSN: 0256-1115
eISSN: 1975-7220

Designing an atmosphere controlling hollow fiber membrane system for mango preservation

Hong Liu, Linxiang Fu, Huan Liu, Caili Zhang, Bing Cao, and Pei Li†

College of Materials Science and Engineering, Beijing University of Chemical Technology, Beijing 100029, China
(*Received 14 December 2016 • accepted 5 April 2017*)

Abstract−We devised an atmosphere controlling facility to gain a longer life span for mango. A membrane module made of polyethersulfone/polydimethylsiloxane (PES/PDMS) composite membrane was applied to selectively permeate CO_2 from the gas mixture of the fruit container. To design the membrane separation system, two models were introduced into our mathematical simulations: (1) an equilibrium model giving the optimal membrane area, the compositions of CO_2 and O_2 in the fruit container, feed flow rate and pressures on both the feed and permeate sides of the module, and (2) a dynamic model simulating the change in the gas composition of the fruit container with time. The pressure build-up in the bore side of the hollow fiber was also discussed using the Hagen-Poiseuille equation. The best membrane module configuration was obtained based on the pressure build-up analysis. That was (1) the vacuum pressure should be set at 0.1 bar, (2) the hollow fiber inner diameter should be 0.45 mm, and (3) the vacuum should be applied at both ends of the hollow fiber bore sides.

Keywords: Membranes, Coatings, Application, Fibers, Separation Techniques

INTRODUCTION

Mangoes are delicious but if not stored properly they can easily deteriorate. Until now, knowledge about the potential shelf life, quality changes or microbial population of fresh-cut mangos has been limited [1]. To be able to design and operate a van container that can prolong the mango's shelf life, factors such as biological effects of temperature, relative humidity, modified oxygen and carbon dioxide levels need to be controlled precisely [2,3]. In general, exposure to concentrated O_2 alone cannot inhibit microbial growth effectively, while in most cases, high CO_2 concentration may reduce the growth of bacteria to some extent [4]. So it is important to control the gas composition. Currently, there are two main modified atmosphere (MA) implementations being used commercially: (1) controlled atmosphere storage (CAS), and (2) modified atmosphere storage (MAP) [5]. MAP is beneficial for minimally processed products as reported by Amanatidou and others [6-9]. While, CAS is more appropriate and practical for large-scale perishable transport [5,10]. In recent years, energy efficient membrane-based technology has become one of the most important separation processes [11,12]. Compared to other gas separation techniques [13, 14], membrane separation has advantages such as low operation price, high efficiency, and environmental benign [15,16]. Chong et al. [5] designed a membrane-controlled atmosphere storage (MCAS) system. Their work has enlightened us in the designation of the MCAS system for mango reservation. However, since the preferred storage condition for mango is very different from the avocado used in their system, many adjustments have to be made in our designs which will be introduced in detail in this work.

According to the data given by Ravindra and Goswami, mango should be stored at 13 °C and normal pressure, with a relative humidity of 85-90%, and an gas composition of O_2 at 3-5%, CO_2 at 5-8% and N_2 at 87-92% [17]. Under this condition, the respiration rate of mango is limited to 0.2544 (m^3/h). In our design, the temperature of the mango reefer is regulated by using a common refrigerator system, while the gas composition is controlled with a membrane-based system. When running the membrane system, certain amount of the gas will pass through the membrane and be discharged to the atmosphere. This will cause a pressure decrease inside the mango reefer. Hence, a pressure balance equipment is installed to maintain a normal pressure inside the mango reefer. The crucial point of designing the membrane system is to precisely remove the CO_2 produced by mango respiration, while at the same time supply O_2 that is required for mango respiration through the pressure balance system. By doing so, a stable gas composition can be obtained. The driving force of a gas separation membrane is the pressure difference between the feed and permeate sides. Note that the relative humidity inside the mango container is 85-90%. Hence, a slightly higher pressure in the membrane feed side will lead to water condensation on the membrane surface, which may swell the membrane material and deteriorate the membrane separation performance. Therefore, to create a driving force, the membrane permeate side has to be vacuumed and the pressure in the feed side is kept at 1 bar. Based on this design, the driving force is less than 1 bar, which is relatively small. Hence, we have to select a material with high gas flux to save the membrane area. In this work, PDMS was chosen for its high CO_2 permeability and moderate CO_2 selectivity over N_2 [18-20]. Since PDMS is a rubbery material, its mechanical strength is weak. We have to prepare a porous substrate to provide the mechanical strength to the membrane. Compared

†To whom correspondence should be addressed.
E-mail: lipei@mail.buct.edu.cn

to other membrane configurations, the hollow fiber membrane offers many advantages [21-24], such as a large effective membrane area per unit volume that will save the space occupied by the membrane module [25]. Therefore, we fabricated a porous hollow fiber membrane using a low-cost material PES with good mechanical and chemical properties, and subsequently, the porous substrate was coated by a very thin PDMS layer that acted as the selective layer. In many studies, polyacrylonitrile (PAN) is selected as the substrate for fabricating PAN/PDMS composite membranes [26, 27]. Here, we chose PES in consideration of its better physical properties such as strength and flexibility compared with PAN [28-30]. Furthermore, PES is a hydrophobic material which makes the PES hollow fiber membrane very stable in humid environment [31,32].

Our objective was to design the required membrane area, hollow fiber module configuration, and operation parameters to meet the best storage condition for mango. To realize this purpose, we developed two models. Through the equilibrium model, we calculated the membrane area and the parameters that fitted the requirement. Using the dynamic model, we simulated the changes in the gas compositions with time. At the end, we discussed the pressure build-up in the bore side and figured out the best membrane module configuration.

MODEL DEVELOPMENT

1. Mathematical Model for Gas Separation

It is essential to figure out the effects of operation parameters on the performance of the membrane module [33,34]; thus, developing a mathematical model for estimating the membrane performance is necessary to design the system. Actually, there are four idealized flow patterns for operation of a membrane gas separation module [5]. Bore side feed may encounter significant pressure build-up along the hollow fiber membrane due to the small dimension of the membrane bore side and high feed flux. While in the shell side feed mode, the pressure build-up of the feed gas is trivial since the hydrodynamic radius of the membrane module is much greater than that of the hollow fiber bore side. Hence, we chose the co-current flow mode, shell side feed hollow fiber permeator and ignored the pressure build-up in the shell side. To simplify the model, we assumed a constant gas composition in the feed side. In this case, there was no difference between the co-current flow and the counter-current flow modes. Wang et al. [35] built a model to characterize the separation performance of hollow fiber membrane that separated a binary gas mixture. They also studied the effects of pressure drop, concentration polarization and non-ideal gas behavior for binary gas separations. We used their model to analyze the separation performance of our hollow fiber module for separating a CO_2, O_2 and N_2 ternary gas mixture.

2. Equilibrium Model

To build an equilibrium model, we considered the system already reached steady state with a preferred gas composition. That meant the concentrations of O_2 and CO_2 both reached 5%, respectively. To maintain a normal pressure inside the container, the gas flowing back to the container included two parts: retentate flow from membrane module, and supplementary gas from the pressure balance system. The composition of the supplementary gas was O_2 21%, N_2 79%, and CO_2 0%, which was equal to the typical air composition. And the overall composition of the two flows was supposed to be O_2 5%, CO_2 5%, and N_2 90% to maintain the preferred gas composition inside the container. Since it was difficult to directly calculate the membrane area and operation parameters to maintain both the concentrations of O_2 and CO_2, we first targeted to control the CO_2 concentration inside the container. Based on the modeling results, a series of solutions of which a specific membrane area with operational parameters could meet the requirement of controlling the CO_2 concentration were obtained. Then, we tested the relative O_2 concentration of each solution and picked the solutions that could satisfy the concentration requirements of both gases. The key points were (1) the CO_2 generated by the mango needed to be discharged by the membrane, (2) the O_2 consumed by the mango which was the same amount as the produced CO_2 needed to be supplied by the outside atmosphere, and (3) the above two processes took place at the same moment. Therefore, the CO_2 permeate rate (Q_{p1}) was the same as the CO_2 generation rate, which was the mango's respiration rate. Then we could calculate the membrane area and feed flow rate (Q_f) through the equilibrium model, but those results only met the requirement of CO_2 removal. To maintain the concentration of O_2, we had to consider the permeate flow and the supplementary air at the same time, and made an optimal choice from the results we obtained to meet the concentration requirements for both gases.

Jin et al. [36] analyzed the effect of stage cut on the separation performance of a binary gas system, but did not apply the model to ternary gas systems. Chong et al. [5] developed a mathematical model for ternary gas separation, and we utilized a similar method to build our mathematical model. In this model, stage cut, which is defined as the ratio of the overall permeate flow rate to the overall feed flow rate, was emphasized. The mathematical model of the separation of multicomponent gas by a hollow fiber membrane module is relatively complicated. So, we made several assumptions to simplify the process for ternary gas separation:

(1) Steady state operation,

(2) Ignoring the pressure build-up in the shell side and bore side,

(3) Ignoring the concentration polarization.

And several equations used to describe this model are given as follows:

The overall mass balance is given by Eq. (1):

$$Q_f = Q_r + Q_p \tag{1}$$

where Q_f is the feed flow rate (m^3/h), Q_r the retentate flow rate (m^3/h), and Q_p the permeate flow rate (m^3/h). The overall mass balance for single component of the gas mixture is described in Eq. (2):

$$Q_f x_{fi} = Q_r x_{ri} + Q_p y_{pi} \tag{2}$$

where "i" represents different component (1=CO_2, 2=O_2, 3=N_2). In a membrane separation process, the faster permeating species are concentrated in the permeate side, while the slower permeate are concentrated in the retentate. The stage cut (θ) is defined as Eq. (3):

$$\theta = \frac{Q_p}{Q_f} \tag{3}$$

Substituting Eq. (3) into Eq. (2) gives Eq. (4):

$$x_{ri}=\frac{x_{fi}-\theta y_{pi}}{1-\theta} \quad (4)$$

where "i" represents different component (1=CO_2, 2=O_2, 3=N_2).

The basic mass transfer equation of the gas membrane is:

$$Q_{pi}=AP_i\nabla P$$

where P_i refers to the permeance (cm^3(STP)/(cm^2 s bar)) of the specified component ∇P refers to the pressure difference (bar), so the permeation rates of the gas can be described as Eq. (5):

$$Q_{pi}=Q_p y_{pi}=AP_i(P_H x_{ri}-P_L y_{pi}) \quad (5)$$

P_H and P_L represent for the pressure at retentate and permeate sides, respectively (bar).

And the mole fraction of gas "i" in permeate flow is given by Eq. (6):

$$y_{pi}=\frac{Q_{pi}}{Q_{p1}+Q_{p2}+Q_{p3}} \quad (6)$$

To cut down the unknown parameters, the permeation rate of N_2 is expressed by the parameters of O_2 and CO_2 as described in Eq. (7):

$$Q_{p3}=Q_p(1-y_{p1}-y_{p2})=AP_3[P_H(1-x_{r1}-x_{r2})-P_L(1-y_{p1}-y_{p2})] \quad (7)$$

Then, by substituting different components (1 and 2) in Eq. (4) and (5) into Eq. (6), we get two quadratic Eqs. (8) and (9).

$$a_1y_{p1}^2+b_1y_{p1}+c_1=0 \quad (8)$$

$$a_2y_{p2}^2+b_2y_{p2}+c_2=0 \quad (9)$$

where

$$a_1=(P_3-P_1)[r(1-\theta)+\theta],\ a_2=(P_3-P_2)[r(1-\theta)+\theta];$$
$$b_1=P_1[x_{f1}+r(1-\theta)+\theta]+P_2[x_{f2}-y_{p2}r(1-\theta)-y_{p2}\theta]$$
$$+P_3[(1-r)(1-\theta)-x_{f1}-x_{f2}+y_{p2}\theta+y_{p2}r(1-\theta)]$$
$$b_2=P_1[x_{f1}-y_{p1}r(1-\theta)-y_{p1}\theta]+P_2[x_{f2}+r(1-\theta)+\theta]$$
$$+P_3[(1-r)(1-\theta)-x_{f1}-x_{f2}+y_{p1}\theta+y_{p1}r(1-\theta)]$$
$$c_1=-P_1x_{f1},\ c_2=-P_2x_{f2}$$

P_i (i=1, 2, 3) represents pure gas flux (listed in Table 1) in units of GPU for the PES/PDMS hollow fiber membrane.

We set CO_2 concentration, x_{f1}, and O_2 concentration, x_{f2} to be 5%. Eqs. (8) and (9) can be solved by Newton's iteration method by giving reasonable values of θ, pressure ratio r (r=P_L/P_H) and the composition of feed flow, and the result shows the composition of permeate side including y_{p1}, y_{p2}, and y_{p3}. We set the different values of θ from 0.1-0.5, and pressure ratio r from 0.1 to 0.2. If one of them is fixed, we could obtain a series of results by varying the other parameters. Note that all results meet the requirement of removal CO_2 generated by mango respiration. By solving Eqs. (8) and (9), we get y_{p1} and y_{p2}, the mole fraction of CO_2 and O_2 in permeate flow. Then we can further determine the mole fractions of CO_2 and O_2 in the retentate flow x_{r1}, x_{r2} using Eq. (4). Furthermore, by inputting all the values to Eq. (5), the membrane area that meets the requirement to maintain the concentration of CO_2 is acquired. Values of Q_p and Q_f are determined by using Eqs. (6) and (3), respectively. The overall O_2 concentration of the flow back to the container is estimated by using Eq. (10):

$$Q_f x_{f2}=Q_r x_{r2}+Q_p y_{p2}+Q_{sp} y_{sp2} \quad (10)$$

where Q_{sp} represents the supplied air flow rate; the concentration of O_2, y_{sp2} is a constant value of 0.21. Thus, we can calculate the concentration of O_2 when the system reaches equilibrium.

Table 1. Pure gas permeance of the PES/PDMS hollow fiber membrane (estimated)

Pure gas	Permeance (GPU)
CO_2	1000
O_2	200
N_2	100

1 GPU=10^{-6} cm^3 (STP)/(cm^2 s cm Hg)

3. Dynamic Model

We have already obtained a number of solutions, each of which includes membrane area and operational parameters. However, when a solution with fixed membrane area A, Q_f, and r is applied to a system of which the gas composition is not at the equilibrium stage, the stage cut (θ) will change with time. Thus, we introduce a dynamic model to analyze this process. The dynamic model assumes that within a short time interval, Δt, which in our module is one hour, the composition of the gas inside the container is regarded as a constant. That is, within one hour, the system fits the equilibrium model assumption. Then, the whole gas separation process can be divided into many ideal periods (Δt) that fit the description. And if we accumulate those periods, the relation of gas composition with time is obtained.

Specifically, when the membrane area (A), feed flow rate (Q_f) and pressure ratio (r) were settled, the parameters of the first period were expressed as $\theta^{1'}$, $Q_p^{1'}$, $y_{p1}^{1'}$, $y_{p2}^{1'}$. To calculate the values of stage cut and gas composition of the first period, we set a guess value of initial stage cut $\theta 1^0$, and the compositions $x_{f1}1^0$, $x_{f2}1^0$ in the feed were the same as the initial concentrations of O_2, and CO_2 inside the container. Hence, we could calculate $y_{p1}1^0$, $y_{p2}1^0$ in this period through Eqs. (7), and (8), and subsequently obtained Q_p1^0 by substituting $y_{p1}1^0$ or $y_{p2}1^0$ into Eqs. (4) and (5). Then, a new value of stage cut $\theta 1^1$ could be calculated since $\theta 1^1=Q_p1^0/Q_f$. Substituting $\theta 1^1$ into Eqs. (7), and (8) gave a set of new values for $y_{p1}1^1$, $y_{p2}1^1$ which could be used to calculate $\theta 1^2$ through the same calculation procedure. Repeating this process till $\theta 1^n=\theta 1^{n+1}$, the convergent stage cut $\theta 1'$ was obtained and the corresponding values of Q_p1', $y_{p1}1'$, and $y_{p2}1'$ were applied to calculate the gas composition inside the container ($x_{f1}1^1$, $x_{f2}1^1$) by using Eq. (11).

$$x_{fi}^{n+1}=x_{fi}^n+(r_i+Q_{sp}x_{spi}-Q_p y_{pi})\Delta t/V \ (n=0, 1, 2, 3\ \ldots) \quad (11)$$

where "i" represents different components (1=CO_2, 2=O_2, 3=N_2). These two values ($x_{f1}1^1$ and $x_{f2}1^1$) were used to calculate the stage cut and other parameters for the next operation period. By repeating this method for certain periods, the changes in the gas composition inside the container with time were acquired.

PRESSURE BUILD-UP IN THE MEMBRANE BORE SIDE

In the above models, we assumed negligible pressure build-ups in both membrane shell and bore sides. However, the diameter of

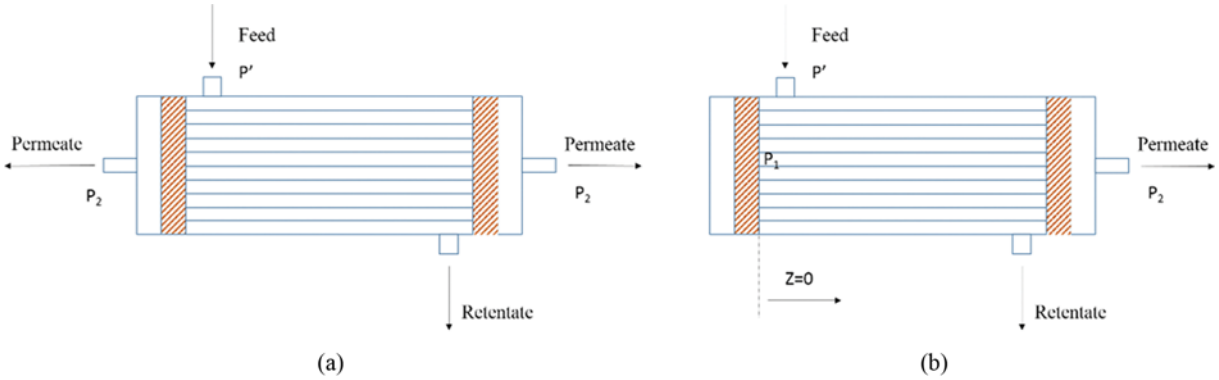

Fig. 1. Hollow fiber membrane module configurations: (a) one side out and one side sealed; (b) two-side out.

hollow fiber membrane was so small that the pressure build-up in bore side was not trivial and would lead to insufficient driving force for the membrane module to be able to remove all CO_2 [37]. As shown in Fig. 1, we analyzed two membrane configurations which were one-side out and one side sealed module (Fig. 1(a)) and two-side out module (Fig. 1(b)). To simplify the calculations, we made several assumptions: (1) the pressure build-up in the fiber bore side followed Hagen-Poiseuille equation for compressible fluid; (2) negligible concentration polarization in both the fiber shell and bore sides; and (3) negligible pressure build-up in the fiber shell side.

1. Basic Equations

The Hagen-Poiseuille equation for compressible fluid was used to describe the pressure build-up in the bore side of a hollow fiber as shown in Eq. (12):

$$\frac{dP_l}{dz} = -\frac{8\mu RTq_p}{\pi P_l r_i^4 N} \tag{12}$$

where P_l is the pressure of the sealed side, r_i the fiber inner radius (m), T the operating temperature (K), Z the length along the permeator, R the gas constant, and μ the gas viscosity (bar·s). We used Eq. (13) for calculating the permeate flowrate:

$$q_p = p_g \pi D(P' - P_l)NZ \tag{13}$$

where P′ refers to the pressure of the feed gas (kept at 1 bar). We substituted Eq. (13) into Eq. (12), and set the boundary conditions as: at Z=0, Pl=P1, (P1 corresponding to the highest pressure in the hollow fiber module). Then it gives the following Eq. (14):

$$P_l - P_2 + P' \ln\frac{P' - P_l}{P' - P_2} = -\frac{8\mu RTP_g}{r_i^4} Z^2 \tag{14}$$

If the length of the module and the vacuum pressure are known, we can calculate the pressure distribution along the fiber. After that, using Eq. (13), we can estimate the number of hollow fibers in the membrane module. Based on this method, the pressure build-up for both one-side out and two-side out hollow fiber modules were analyzed.

RESULTS AND DISCUSSIONS

1. The Effects of Stage Cut and Permeate Side Pressure on the O_2 Concentration in the Mango Container

According to our equilibrium model, the membrane area and operation parameters are calculated to meet the requirement for removing all CO_2. Then the resulting O_2 concentration (x_{f2}) inside the mango container is estimated using Eq. (10). Obviously, we have to make sure that the concentration of O_2 (x_{f2}) stays in the target range (3-5%). During the calculation process, we obtained a series of data including the membrane area and concentration of O_2 back to container by changing the values of θ and/or pressure ratio r. The results are shown in Fig. 2 and Fig. 3.

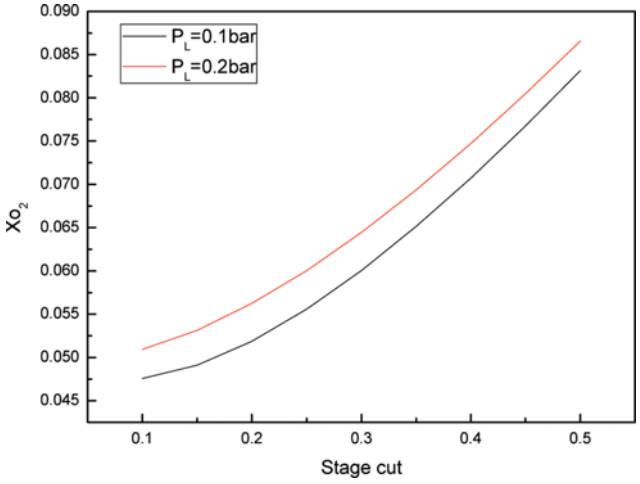

Fig. 2. Calculated concentration of O_2 inside the reefer changes with stage cut under different pressure.

Fig. 2 shows that the O_2 concentration can be controlled below 5% only when the stage cut is lower than 0.2. And the lower the pressure of the permeate side, the smaller the O_2 concentration can be got inside the container. Under the same permeate pressure, the concentration of O_2 increases with the stage cut. It is because a higher stage cut indicates more N_2 permeate through the membrane with CO_2. When this happens, more supplied gas is required to balance the pressure inside the container. Since the O_2 concentration in supplied gas is 0.21, which is much higher than the O_2 concentration inside the container (5%), it will lead to an increase in the O_2 concentration. Under the same stage cut, the concentration of O_2 increases with the permeate pressure. This can be explained by the changes in the membrane driving forces. As the permeate pressure increases from 0.1 bar to 0.2 bar, the driving

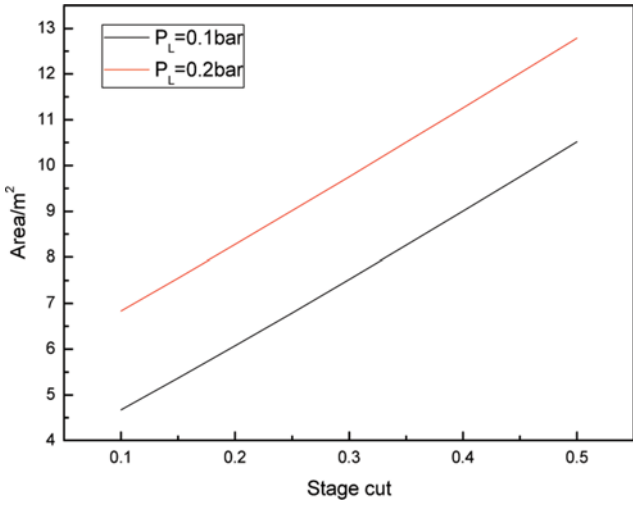

Fig. 3. The changes of membrane area with stage cut under different permeate pressures.

force for CO_2 is greatly reduced since the mole fraction of CO_2 in the feed side is only 5%. But this effect is relatively mild for N_2 since the mole fraction of N_2 is 90%. Hence, more N_2 will transport to membrane permeate side if same amount of CO_2 needs to be separated. It will again lead to a greater amount of O_2 enriched supplied gas being introduced to the container and increasing the O_2 concentration.

Fig. 3 shows that the membrane area decreases as the stage cut and/or the permeate pressure is reduced. As the stage cut decreases, the feed flow rate increases. Hence, the CO_2 concentration in the feed is high, which leads to a greater CO_2 driving force. And less membrane area is required to remove all CO_2. When the permeate side pressure is reduced, the driving force for CO_2 increases significantly. Therefore, the demanded membrane area is decreased.

2. The Effect of Permeate Side Pressure on the Membrane Module Parameters

In this study, the membrane driving force can only be enhanced by applying a higher vacuum on the permeate side to avoid water condensation on the membrane feed side. However, a pressure infinitely approaching absolute vacuum is costly in practice. In industrial applications, the applicable vacuum range is from 0.1-0.2 bar [38]. Therefore, we preset the permeate side pressures at 0.1 bar and 0.2 bar, respectively, to estimate the values of the rest of membrane module parameters and analyze the pressure impacts.

Table 2 lists the parameters of two membrane modules. Both two modules fulfill the requirements since both CO_2 and O_2 concentrations are well controlled at 5%. Only the permeate side pressures are preset, other parameters including stage cut, feed flow rate, permeate flow rate, and membrane area are obtained by model simulation to achieve the stabilized O_2 and CO_2 concentrations of 5%. An interesting observation is that the membrane areas and permeate flow rates of the two membrane modules are very similar. The main differences between these two designs lie in the feed flow rate and stage cut. Membranes with a higher permeate side pressure need a greater feed flow rate. Note that the key of the design is to control the O_2 concentration as well as the CO_2 concentration. Since the supplied gas flow rate should be equal to the permeate gas flow rate, the same permeate flow rate of the two membrane modules has to be realized to control the same O_2 concentration of the mango container. Therefore, as the permeate flow rate is fixed, a higher feed flow rate is required when membrane module is operated with a higher permeate side pressure. Because with a high feed flow rate, the CO_2 partial pressure in the feed is higher, since less amount of CO_2 is passing through the membrane. And the increase in the CO_2 concentration in the feed will comprise the increase in the permeate side pressure so that maintain the CO_2 driving force of the membrane.

3. Dynamic Simulation

Fig. 4 shows the changes in the gas concentrations inside the mango container with time using membrane module one and two whose parameters are listed in Table 2. When the initial composition of the gas inside the container was N_2 78%, O_2 21%, CO_2 0.1%, the preferred gas composition (O_2=5%, CO_2=5%) could be realized after running the membrane system for 60 hours at both two permeate pressures. As can be seen, when membrane permeate pressure is lower (0.1 bar), the feed flow rate is significantly reduced, which may save energy for the feed gas blower.

Fig. 5 shows the changes in the gas composition in an airtight mango container system. It is obvious that the concentration of O_2 drops significantly without air control system, and after 33 hours the O_2 is depleted. Under this situation, the mango will undergo anaerobic respiration and produce lactic acid, which makes the mango flavor become sour and distasteful. Therefore, an atmosphere controlling system is necessary.

Table 2. Parameters of two membrane modules

Module parameters	Module one	Module two
Pressure of permeate side (P_L/bar)	0.1	0.2
Stage cut θ (at equilibrium)	0.2	0.1
CO_2 mole fraction (at equilibrium)	0.05	0.05
Flow rate feed to membrane (m^3/h)	9.44	18.88
Permeate flow rate (m^3/h)	1.89	1.89
Membrane area (m^2)	6.07	6.83
O_2 mole fraction (at equilibrium)	0.05	0.05
Outer diameter of the fiber (mm)	0.65	0.65
Number of fiber (one end outlet and one end sealed)	3445	3775

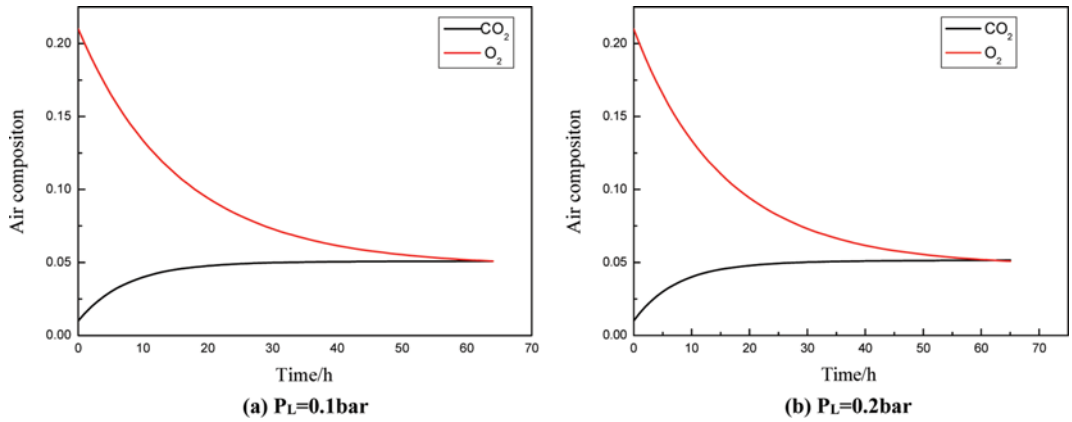

Fig. 4. Changes in the O_2 and CO_2 concentrations of the container with time under different permeate pressures (initial concentrations: O_2= 0.21, CO_2=0.01).

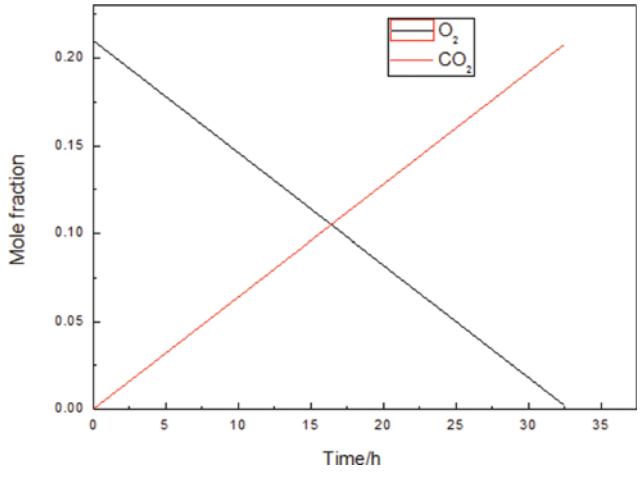

Fig. 5. The gas composition changes with time in an airtight container without the membrane separation system.

4. Effects of Hollow Fiber Dimensions on Pressure Build-up in the Fiber Bore Side

Table 3 lists the dimensions of the PES/PDMS hollow fiber membranes. Since the inner diameters of hollow fiber membranes are relatively small, the pressure build-up along the hollow fiber bore sides cannot be ignored. Therefore, the pressure distribution inside the hollow fiber bore side is estimated by using the Hagen-Poiseuille equation and shown in Fig. 6. For the module with one side out and one side sealed configuration, when the inner diameter of fiber decreases, the pressure build-up increases. The largest increases in the hollow fiber bore sides are obtained at the sealed end of the hollow fibers, which are 0.12, 0.15, and 0.20 bar, respectively, corresponding to the hollow fiber inner diameters of 0.45, 0.40, and 0.35 mm, respectively, as shown in Fig. 6(a). Similar results are shown in Fig. 6(b) of which the pressure build-up is 0.07, 0.10, and 0.13 bar for fiber inner diameters of 0.45, 0.40, and 0.35 mm, respectively. Therefore, a larger fiber inner diameter results in less pressure buildup.

An interesting phenomenon was observed: as the permeate side pressure increased from 0.1 to 0.2 bar, the pressure build-up was greatly reduced. This can be explained according to Eq. (12) and Table 2. When the permeate pressure increases to 0.2 bar, the number of fibers increases from 3445 to 3775. More hollow fibers result in less gas flow rate of each hollow fiber, which leads to small pressure build-up. In addition, based on Eq. (12), as the vacuum pressure increases to 0.2 bar, the denominator in the right side increases and hence dP_i/dz decreases, which means the pressure build-up decreases.

Since the pressure build-up at the fiber bore side is large, this

Table 3. Dimensions of the hollow fiber composite membranes

Membrane material	Polyethersulfone/polydimethylsiloxane
Inner diameter of fiber	0.35 mm/0.40 mm/0.45 mm
Outer diameter of fiber	0.65 mm/0.70 mm/0.66 mm
Number of fibers	2900-4200
Membrane effective length	1.0 m
Stage cut	0.1 to 0.5
Temperature	286.15 K (13 °C)
Mixed gas	
Oxygen/carbon dioxide/nitrogen	5/5/90
Upstream pressure	1 bar
Downstream pressure	0.1 bar or 0.2 bar

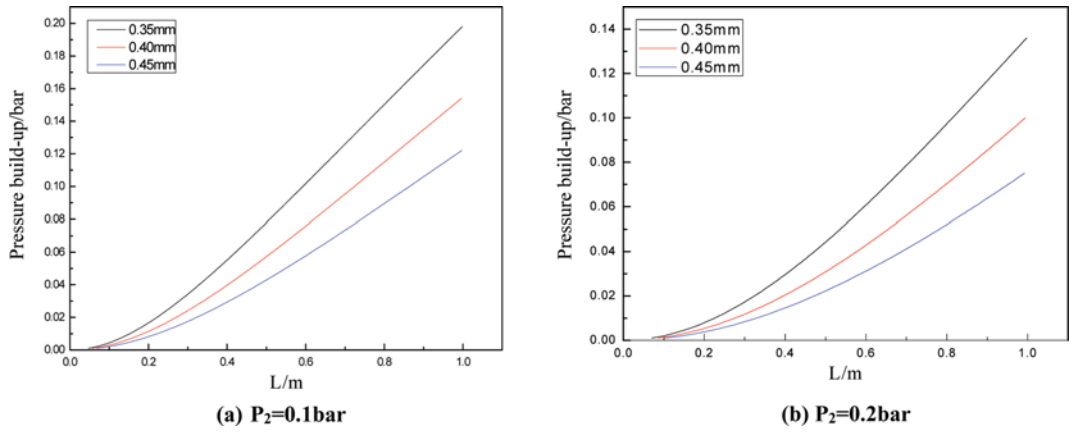

Fig. 6. Effect of hollow fiber length (L) on pressure build-up (the hollow fiber module is one end outlet and one end sealed) (a) P_2=0.1 bar (b) P_2=0.2 bar.

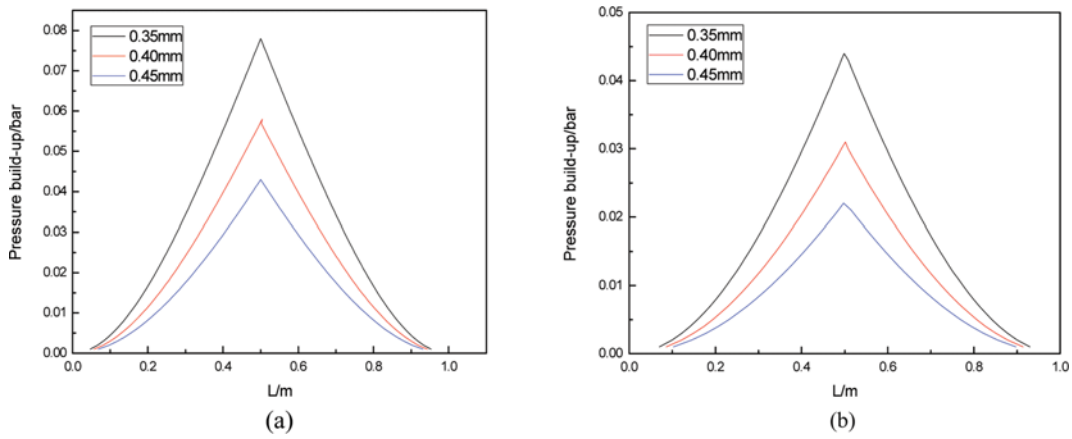

Fig. 7. Pressure distributions for two-side out hollow fiber module: (a) The vacuum pressure is 0.1 bar; and (b) the vacuum pressure is 0.2 bar.

seriously reduces the membrane driving force. The two-sides out configuration should be adopted because this design reduces the path length of the permeate gas by half. Fig. 7 shows the pressure distributions of the two-side out hollow fiber membranes. As can be seen, the biggest pressure build-up is located in the middle of the hollow fiber membrane, which is only half of the value of the one-side out configuration. With this design, the average pressure in the bore side is 0.12 bar when hollow fiber membrane has an inner diameter of 0.45 mm and the pressure of the vacuum pump is 0.1 bar. In this case, the driving force should be very similar to the designed value. Therefore, the best hollow fiber module design is: (1) 0.1 bar of the vacuum pressure, (2) 0.45 mm of the hollow fiber inner diameter, and (3) two-side out of the hollow fiber bore side.

CONCLUSIONS

We have developed a mathematical model to describe membrane separation for a ternary mixed gas system and applied it in a membrane based atmospheric controlling system. The pressure ratio of the membrane upstream to downstream, stage cut and membrane area that met the requirements for maintaining the preferred gas compositions in the mango container were obtained. A dynamic model was also established to analyze the changes in the gas composition with time inside the container. The best hollow fiber configuration was obtained after analyzing the pressure build-up at the hollow fiber bore side using the Hagen-Poiseuille equation for compressible fluid.

ACKNOWLEDGEMENTS

The authors would like to thank the National Natural Science Foundation of China (contract grant number 51403012), the State Key Laboratory of Organic-Inorganic Composites of Beijing University of Chemical Technology (contract grant number 22010006013), and the Fundamental Research Funds for the Central Universities (contract grant number buctrc201415) for funding this study.

NOMENCLATURE

A : membrane area [m^2]
P_i : pure gas permeabilities of gas i [m^3 (STP)/(m^2 s bar)]
P_H, P_L : pressure at retentate and permeate sides, respectively [bar]
Q_f : feed flow rate to membrane module [m^3/h]

Q_{sp} : flowrate of gas feed back to the reefer [m^3/h]
Q_s : sweep flowrate from membrane module [m^3/h]
Q_p : permeate flowrate from membrane module [m^3/h]
Q_r : retentate flowrate from membrane module [m^3/h]
r : pressure ratio, P_L/P_H
R_i : generation rate of gas i [m^3/h]
V : volume of the reefer [m^3]
x_i : mole fraction of gas i in the reefer
x_{fi} : mole fraction of gas i in feed to membrane module
x_{spi} : mole fraction of gas i in gas feed back to the reefer
x_{si} : mole fraction of gas i in sweep flow
x_{ri} : mole fraction of gas i in retentate flow
y_{pi} : mole fraction of gas i in permeate flow
Δt : time interval [h]
R : gas constant, 3.711×10^{-3} [bar m^3/(m^3(STP)K)]
Z : length of the module [m]
N : number of the hollow fiber
r_i : inner diameter of the hollow fiber [m]

Greek Letters

θ : stage cut, Q_p/Q_f
viscosity of the gas, 5.117×10^{-14} [bar h]

REFERENCES

1. N. Rattanapanone, Y. Lee, T. X. Wu and A. E. Watada, *Hortscience*., **36**, 1091 (2001).
2. J. M. Harvey, *Int. J. Refrig*., **4**, 293 (1981).
3. J. Poubol and H. Izumi, *J. Food Sci*., **70**, M69 (2005).
4. A. Amanatidou, E. J. Smid and L. G. M. Gorris, *J. Appl. Microbiol*., **86**, 429 (1999).
5. K. L.Chong, N. Peng, H. Yin, G. G. Lipscomb and T.-S. Chung, *J. Food Eng*., **114**, 61 (2013).
6. M. Martínez-Ferrer, C. Harper, F. Pérez-Muntoz and M. Chaparro, *J. Food Sci*., **67**, 3365 (2002).
7. R. F. Artés, Villaescusa and J. A. Tudela, *J. Food Sci*., **65**, 1112 (2000).
8. A. Amanatidou, R. A. Slump, L. G. M. Gorris and E. J. Smid, *J. Food Sci*., **65**, 61 (2000).
9. K. Tano, J. Arul, G. Doyon and F. Castaigne, *J. Food Sci*., **64**, 1073 (1999).
10. S. C. Fonseca, F. A. Oliveira and J. K. Brecht, *J. Food Eng*., **52**, 99 (2002).
11. P. Bernardo, E. Drioli and G. Golemme, *Ind. Eng. Chem. Res*., **48**, 4638 (2009).
12. M. Binns, S.-Y. Oh, D.-H. Kwak and J.-K. Kim, *Korean J. Chem. Eng*., **32**, 383 (2015).
13. K. K. Sirkar, *Chem. Eng. Sci*., **32**, 1137 (1977).
14. S. Alexander Stern, *J. Membr. Sci*., **94**, 1 (1994).
15. F. Ahmad, K. K. Lau, S. S. M. Lock, S. Rafiq, A. U. Khan and M. Lee, *J. Ind. Eng. Chem. (Amsterdam, Neth.)*, **21**, 1246 (2015).
16. S. S. Hosseini, J. A. Dehkordi and P. K. Kundu, *Korean J. Chem. Eng*., **33**, 3085 (2016).
17. M. R.Ravindra and T. K.Goswami, *Biosyst. Eng*., **99**, 239 (2008).
18. F. W. Wu, L. Li, Z. H. Xu, S. J. Tan and Z. B. Zhang, *Chem. Eng. J. (Amsterdam, Neth.)*, **117**, 51 (2006).
19. T. Hu, G. X. Dong, H. Y. Li and V. Chen, *J. Membr. Sci*., **432**, 13 (2013).
20. D. Sun, P. Yang, L. Lin, H.-H. Yang and B.-B. Li, *Korean J. Chem. Eng*., **31**, 1877 (2014).
21. R. Khalilpour, A. Abbas, Z. Lai and I. Pinnau, *Chem. Eng. Res. Des*., **91**, 332 (2013).
22. F. Ahmad, K. K. Lau, A. M. Shariff and Y. Fong Yeong, *J. Membr. Sci*., **430**, 44 (2013).
23. P. Li and M. R. Coleman., *Eur. Polym. J*., **49**, 482 (2013).
24. P. Li, T. S. Chung and D. R. Paul, *J. Membr. Sci*., **450**, 380 (2014).
25. N. Peng, N. Widjojo, P. Sukitpaneenit, M. M. Teoh, G. G. Lipscomb, T.-S. Chung and J.-Y. Lai, *Prog. Polym. Sci*., **37**, 1401 (2012).
26. P. Li, H. Z. Chen and T.-S. Chung, *J. Membr. Sci*., **434**,18 (2013).
27. H. Z. Chen, Z. Thong, P. Li and T.-S. Chung, *Int. J. Hydrogen. Energy*, **39**, 5043 (2014).
28. S. S. Madaeni, E. Enayati and V. Vatanpour, *J. Appl. Polym. Sci*., **122**, 827 (2011).
29. G. Bakeri, M. Rezaei-DashtArzhandi, A. F. Ismail, T. Matsuura, M. S. Abdullah and N. B. Cheer, *Korean J. Chem. Eng*., **34**, 160 (2017).
30. M. S. Muhamad, M. R. Salim and W. J. Lau, *Korean J. Chem. Eng*., **32**, 2319 (2015).
31. M. Sadrzadeh, M. Amirilargani, K. Shahidi and T. Mohammadi, *J. Membr. Sci*., **342**, 236 (2009).
32. S. A. Sonalkar, P. J. Hao and G. G. Lipscomb, *Ind. Eng. Chem. Res. Res*., **49**, 12074 (2010).
33. V. S. Kovvali, K. R. Krovvidi and A. A. Khan, *J. Membr. Sci*., **73**, 1 (1992).
34. P. J. Hao, J. G. Wijmans, J. Kniep and R. W. Baker, *J. Membr. Sci*., **462**, 131 (2014).
35. R. Wang, S. L. Liu, T. T. Lin and T. S. Chung, *Chem. Eng. Sci*., **57**, 967 (2002).
36. H. G. Jin, S. H. Han, Y. M. Lee and Y. K. Yeo, *Korean J. Chem. Eng*., **28**, 41 (2011).
37. P. Shao and R. Y. M. Huang, *J. Membr. Sci*., **271**, 69 (2006).
38. T. C. Merkel, H. Q. Lin, X. T. Wei and R. Baker, *J. Membr. Sci*., **359**, 126 (2010).